EFFICIENT COMPUTATION OF ELECTRICAL LASLETT COEFFICIENTS FOR ROUNDED-RECTANGULAR PIPES

STEFANIA PETRACCA [a,*], VINCENZO GALDI [b] and INNOCENZO M. PINTO [b]

[a] *Dipartimento di Scienze Fisiche E.R. Caianiello, University of Salerno, via S. Allende, I-84081 Baronissi (SA), Italy;* [b] *Dipartimento di Ingegneria dell'Informazione ed Ingegneria Elettrica, University of Salerno, via Ponte don Melillo, I-84084 Fisciano (SA), Italy*

We present an effective numerical technique for computing the electrical image coefficients for rounded rectangular pipes with perfectly conducting walls. The method of moments is used to solve the involved boundary-value problem in integral form, by means of (a rapidly converging representation of) the rectangular-domain Green's function, together with a set of piecewise parabolic subdomain basis functions, yielding high speed and accuracy, with minimum storage budget (no prior meshing required). As a distinctive feature of the proposed method *no* numerical differentiation is required, resulting into far better accuracy as compared, e.g., to finite-element and finite-difference methods. Application to some simplified cross section geometries relevant to LHC (square with rounded corners, stadium and cut-circle) are presented. As a check of accuracy of the proposed approach, a comparison with available exact (analytical) results for the circular pipe (hardest possible benchmark), shows an excellent agreement.

Keywords: Space charge effect; Tune shift; Numerical method

1 INTRODUCTION

The computation of Laslett coefficients is an important issue in the design of particle accelerators.[1] These coefficients represent the effect of

---

* Corresponding author. E-mail: Stefania.Petracca@cern.ch.

the *image* fields on (transverse) betatron oscillations, and are thus relevant to beam stability. In this connection, efficient and reliable tools for computing the Laslett coefficients could considerably speed up the pipe design procedure.

In this paper we present a numerical technique for computing the electrical image coefficients for some geometries of interest in connection with LHC.[2] These geometries (rounded-corners square, stadium and cut-circle) are obtained from the rectangular one by perturbing (rounding) part of the boundary.

The proposed approach uses the method of moments (henceforth MoM),[3] to solve the pertinent Poisson boundary-value problem. At variance of other authors[4] we use (a rapidly converging representation of) the rectangular-domain Green's function instead of the usual free-space one to solve the involved integral equation. Thanks to this choice, the (unknown) surface charges in the MoM integral equation exist *only* on the perturbed part of the boundary (rounded corners), instead of the whole (rectangular) boundary, with a substantial reduction in the number of unknowns. Using piecewise-parabolic subdomain basis and test functions further reduces the computational burden.

As a result, the typical size of the (resulting, discrete) problem is 20×20, for three-figure accuracy in the Laslett coefficients. To test the accuracy of the proposed method we applied it to the circular geometry, for which exact analytical results are available. This latter provides the *hardest* possible test case (largest departure from the rectangular geometry). Our numerical results are found to be in excellent agreement with the exact ones.

The paper is organized as follows. In Section 2 we introduce the MoM integral equation formulation. In Section 3 we compute the *image* fields and Laslett coefficients. In Section 4 we discuss a number of aspects related to numerical implementation. In Section 5 we outline the main computational features of the proposed method. In Section 6 we check its accuracy by comparison with known analytical solutions, and present numerical results related to some geometries (rounded-corners square, stadium and cut-circle) relevant to LHC. Concluding remarks follow under Section 7. A number of technical details and calculations are collected in Appendices A and B.

2 FORMULATION

A perfectly conducting rectangular boundary with rounded corners is considered, as shown in Figure 1.

The fields produced by a line charge distribution with (linear) charge density Λ going through the (transverse) beam *center of charge*, whose position will be henceforth denoted as r_b, are determined from an electric potential, satisfying Poisson equation under Dirichlet boundary conditions,[5] viz.:

$$\begin{cases} \nabla_t^2 \Phi(r, r_b) = -4\pi\Lambda\delta(r - r_b), & r \in S_0, \\ \Phi(r, r_b) = 0, & r \in \partial S_0, \end{cases} \tag{1}$$

∇_t^2 being the (transverse) Laplacian. The potential admits an integral representation, in terms of a suitable Green's function g:

$$\Phi(r, r_b) = \int_{\partial S_0} g(r, l)\rho_s(l)\mathrm{d}l + \Lambda g(r, r_b), \tag{2}$$

where ρ_s represents the (unknown) surface charge density on ∂S_0 and l is the arc-length on ∂S_0. Usual numerical strategies (e.g. MoM) require
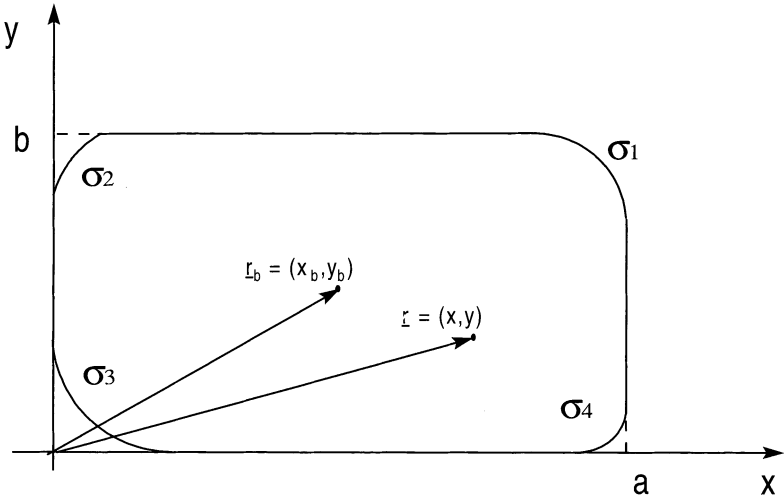

FIGURE 1   Geometry under analysis.

discretization of the surface charge density and/or its expansion on a suitable functional basis on ∂S_0, whose coefficients are determined by solving a linear matrix problem, obtained by enforcing the boundary conditions.[3] In the usual approach g is the *free-space* Green's function g_0:[5]

$$g(\boldsymbol{r}, \boldsymbol{r}_\mathrm{b}) = g_0(\boldsymbol{r}, \boldsymbol{r}_\mathrm{b}) = -2\log|\boldsymbol{r} - \boldsymbol{r}_\mathrm{b}|, \tag{3}$$

and the unknown surface charge density ρ_s is accordingly defined on the *whole* ∂S_0.

A considerable reduction in the problem size is achieved by observing that the geometries of interest (rounded-corners square, stadium and cut-circle) differ from the rectangle only by rounded corners or sides. Then, it might be more advantageous to use the rectangular domain Green's function g_R of the Poisson equation (henceforth RDGF) to recast (2) in the following form:

$$\Phi(\boldsymbol{r}, \boldsymbol{r}_\mathrm{b}) = \sum_k \int_{\sigma_k} g_\mathrm{R}(\boldsymbol{r}, l_k)\rho_{\sigma_k}(l_k)\mathrm{d}l_k + \Lambda g_\mathrm{R}(\boldsymbol{r}, \boldsymbol{r}_\mathrm{b}), \tag{4}$$

where, obviously, the potential given by (4) satisfies already by assumption the boundary conditions on the straight portion of the rectangular contour, and the unknown surface-charge density exists *only* on the rounded portion of ∂S_0, composed by arcs which will be denoted as σ_k (see Figure 1). In (4), l_k denotes the arc-length on σ_k.

Rapidly converging series expansions of the RDGF, which explicitly contain the (logarithmic) singular term are known,[6,7] and are reported in Appendix A.

This formulation allows a substantial memory and CPU time saving.

To solve the integral equation (4), the unknown surface charge densities can be expanded as:

$$\rho_{\sigma_k}(l_k) = \sum_{n=1}^{N} b_n^{(k)} w_n(l_k), \tag{5}$$

where $\boldsymbol{b}^{(k)} = \{b_1^{(k)}, \ldots, b_N^{(k)}\}$, are N-dimensional vectors of unknown coefficients, and $\{w_n(l_k)\}, n = 1, \ldots, N$, is a suitable set of basis functions defined on σ_k. By enforcing the Dirichlet boundary conditions on the

arcs σ_k.

$$\Phi(l_k, \mathbf{r}_b) = 0 \tag{6}$$

is equivalent, in the spirit of Galerkin's procedure,[3] to requiring that

$$\int_{\sigma_k} \Phi(l_k, \mathbf{r}_b) w_n(l_k) \mathrm{d}l_k = 0, \quad n = 1, 2, \ldots, N. \tag{7}$$

The problem can thus be conveniently cast into a block-matrix form:

$$\lfloor L \rfloor \mathbf{b} = \mathbf{c}. \tag{8}$$

Letting P the number of arcs in the rounded portion of the contour ∂S_0, the system (8) is of rank NP. Specifically,

$$\mathbf{c} = \begin{bmatrix} \mathbf{c}^{(1)} \\ \mathbf{c}^{(2)} \\ \vdots \\ \mathbf{c}^{(P)} \end{bmatrix}, \tag{9}$$

where

$$c_i^{(k)} = -\Lambda \int_{\sigma_k} w_i(l_k) g_R(l_k, \mathbf{r}_b) \mathrm{d}l_k, \quad i = 1, \ldots, N; \quad k = 1, \ldots, P, \tag{10}$$

$$\mathbf{b} = \begin{bmatrix} \mathbf{b}^{(1)} \\ \mathbf{b}^{(2)} \\ \vdots \\ \mathbf{b}^{(P)} \end{bmatrix}, \tag{11}$$

where the unknown expansion coefficients $b_i^{(k)}$ are defined by (5), and

$$[L] = \begin{bmatrix} [L_S^{(1)}] & [L_M^{(1,2)}] & \cdots & [L_M^{(1,P)}] \\ [L_M^{(1,2)}] & [L_S^{(2)}] & \cdots & [L_M^{(2,P)}] \\ \vdots & \vdots & \ddots & \vdots \\ [L_M^{(1,P)}] & [L_M^{(2,P)}] & \cdots & [L_S^{(P)}] \end{bmatrix}, \tag{12}$$

where

$$[L_S^{(k)}]_{ij} = \int_{\sigma_k} \int_{\sigma_k} g_R(l_k, l_k') w_i(l_k) w_j(l_k') \mathrm{d}l_k \, \mathrm{d}l_k',$$

$$i,j = 1, \ldots, N, \quad k = 1, \ldots, P, \tag{13}$$

$$[L_M^{(p,q)}]_{ij} = \int_{\sigma_p} \int_{\sigma_q} g_R(l_p, l_q) w_i(l_p) w_j(l_q) \mathrm{d}l_p \, \mathrm{d}l_q,$$

$$i,j = 1, \ldots, N, \quad p,q = 1, \ldots, P. \tag{14}$$

The principal diagonal submatrices $L_S^{(k)}$ in the block-matrix L describe self-interactions taking place between points lying on the same rounded arc, k, of ∂S_0.

The remaining submatrices $[L_M^{(p,q)}]$ describe mutual interaction between points located on different arcs, e.g., p, q. Due to RDGF symmetry, the whole block-matrix $[L]$ is easily recognized to be symmetrical. Furthermore, it could be proved that it is also positive definite and hence non-singular.[7]

Having solved the above system, the scalar potential and related quantities, including Laslett coefficients, can be computed using Eq. (4).

3 IMAGE FIELDS AND LASLETT COEFFICIENTS

The electromagnetic field produced by a thin beam in a vacuum chamber can be conveniently split into the sum of two terms:[1]

$$e(r, r_b) = e^{(sp.ch.)}(r, r_b) + e^{(im.)}(r, r_b), \tag{15}$$

where the *space charge* field describes the free-space effect of all other particles in the beam and depends on the transverse charge distribution only. Conversely, the *image* field depends on the boundary shape, representing the effect of the images of the beam. It can be obtained from the whole field by subtracting the free-space term. The beam dynamics is analyzed (usually for small displacements from the equilibrium position) in terms of these fields. Two cases are commonly considered: *incoherent case* (beam center of charge coincident with beam equilibrium position, $r = r_{eq.}$, and test particle displaced thereof, $r \neq r_b$,

single particle effect); *coherent case* (beam center of charge displaced off the equilibrium position, $r \neq r_{eq.}$, and coincident with test particle, $r = r_b$, whole beam effect).

In both cases the general solution for the transverse oscillation of the beam can be written in terms of two *normal modes*, i.e. special solutions where the oscillations in the x, y directions have the same frequency (see Ref. 8, where normal-mode Laslett coefficients are introduced and thoroughly discussed). The effect of the image fields is conveniently described by the so-called *tune-shifts*, i.e. the deviations of the normal mode frequencies from the betatron frequency, which can be factored as

$$\Delta \nu = F \epsilon. \tag{16}$$

Here the factor F depends only on the beam and machine features,

$$F = \frac{-N R r_0}{\pi \beta_0^2 \gamma_0 \nu L^2} \tag{17}$$

N being the total number of particles in the beam, R the machine radius, r_0 the classical particle radius, ν the nominal tune, L the transverse size of the chamber (e.g., its radius), and the factor ϵ is the *image* or *Laslett* coefficient:

$$\epsilon = \frac{L^2}{4\Lambda} \left\{ \frac{\delta_x u_x + \delta_y u_y}{2} \pm \left[\left(\frac{\delta_y u_y - \delta_x u_x}{2} \right)^2 + \delta_x u_x \delta_y u_y \right]^{1/2} \right\}, \tag{18}$$

where $\Lambda = Nq/2\pi R$ is the beam linear charge density

$$\begin{cases} \delta_{x,y} = \partial_{x,y}|_{r=r_b}, & u_{x,y} = e_{x,y}^{(im.)} + e_{x,y}^{(sp.ch.)}, & \text{incoherent case,} \\ \delta_{x,y} = (\partial_{x,y} + \partial_{x_b,y_b})|_{r=r_b}, & u_{x,y} = e_{x,y}^{(im.)}, & \text{coherent case,} \end{cases} \tag{19}$$

and the $\pm$ signs refer to the two normal modes. Accordingly, for computing Laslett coefficients we need the image field derivatives with respect to x, y (incoherent) and x_b, y_b (coherent). These derivatives can be obtained using the results presented in Section 2, together with Cauchy–Riemann equations, yielding

$$\partial_x e_j(r, r_b) = -\partial_y e_l(r, r_b)$$

$$= -\sum_{k,i=1}^{P,N} b_i^{(k)} \int_{\sigma_k} \partial_{xj}^2 g_R(r, l_k) w_i(l_k) dl_k - \Lambda \partial_{xj}^2 g^{(im.)}(r, r_b), \tag{20}$$

$$\partial_{x_b} e_j(\mathbf{r}, \mathbf{r}_b) = -\sum_{k,i=1}^{P,N} d_i^{(k)} \int_{\sigma_k} \partial_j g_R(\mathbf{r}, l_k) w_i(l_k) dl_k - \Lambda \partial_{jx_b}^2 g^{(\text{im.})}(\mathbf{r}, \mathbf{r}_b), \quad (21)$$

$$\partial_{y_b} e_j(\mathbf{r}, \mathbf{r}_b) = -\sum_{k,i=1}^{P,N} f_i^{(k)} \int_{\sigma_k} \partial_j g_R(\mathbf{r}, l_k) w_i(l_k) dl_k - \Lambda \partial_{jy_b}^2 g^{(\text{im.})}(\mathbf{r}, \mathbf{r}_b), \quad (22)$$

where $j, l = x, y$ with $j \neq l$,

$$g^{(\text{im.})}(\mathbf{r}, \mathbf{r}_b) = g_R(\mathbf{r}, \mathbf{r}_b) - g_0(\mathbf{r}, \mathbf{r}_b). \quad (23)$$

The $g^{(\text{im.})}$ derivatives are easily computed analytically, while the $d_i^{(k)}$, $f_i^{(k)}$ coefficients can be evaluated as:

$$\mathbf{d} = [L]^{-1} \partial_{x_b} \mathbf{c}, \quad (24)$$

$$\mathbf{f} = [L]^{-1} \partial_{y_b} \mathbf{c}. \quad (25)$$

Note that, as $\mathbf{r} \to \mathbf{r}_b$, the above expressions contain indeterminate forms $(\infty - \infty)$, appearing in $g^{(\text{im.})}$ derivatives. Analytical evaluations of these limits are reported in Appendix B.

4 NUMERICAL IMPLEMENTATION

In this section we discuss a number of issues, related to the choice of basis and test functions, the computation of the MoM matrices and the numerical solution of the matrix problems.

As previously stated, we used a set of (partially overlapping) piecewise parabolic *subdomain* basis function. It is convenient to relate the local arc-length l_k on σ_k to the local curvature radius R_k through the local angle $\phi^{(k)}$, via $l_k = R_k \phi^{(k)}$ (see Figure 2). Hence (dropping the suffix k for simplicity)

$$w_i(l) = w_i(R\phi) = \frac{\Delta\phi^2 - (\phi - \phi_i)^2}{\Delta\phi^2},$$

$$\phi_i - \Delta\phi(1 - \delta_{i1}) \leq \phi < \phi_i + \Delta\phi(1 - \delta_{iN}), \quad i = 1, 2, \ldots, N, \quad (26)$$
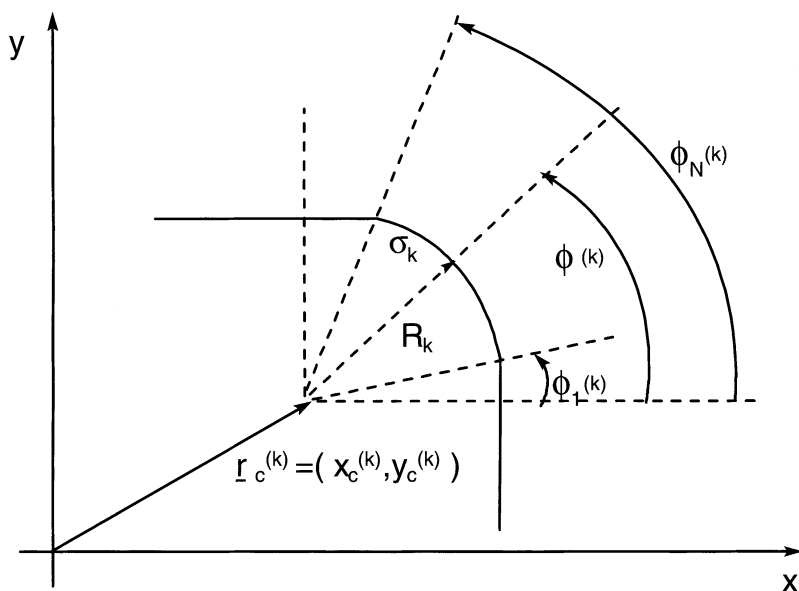
FIGURE 2   Absolute and local coordinate systems.

where $\Delta\phi$ is the angular discretization step (assumed the same for all arcs), and δ_{rs} is the Kronecker symbol[†] (see Figure 3).

This choice yields some benefits. First, *no* polygonal approximation of the arcs is implied, resulting into *fewer* functions being needed for a given accuracy. As a matter of fact, taking $\Delta\phi \sim \pi/10$ was always sufficient to achieve an accuracy better than 0.1% on potentials, fields and Lasletts. Furthermore, the choice of *subdomain* basis functions, rather than *entire-domain* ones, results into a *limited* number of singular integrals[‡] in the computation of $L_S^{(k)}$ elements, due to the (logarithmic) singularity of the RDGF (see Appendix B).

Most integrals (13), (14) and (10) needed to compute the block-matrix L and vectors c, d, f can be evaluated analytically, due to the specially simple form of the chosen basis and test functions. However, there is no significant loss in accuracy or in CPU time in computing the $c_i^{(k)}$, $d_i^{(k)}$,

---

[†] When an extremum lies on the rectangular boundary ($i = 1$, $i = N$) the definition (26) provides the correct behavior of the surface charge density at such a point, where the charge may differ from zero, but its derivative must vanish.

[‡] It is clear from Eq. (13) that singularities may appear only in the presence of an overlap between basis and test functions, which, in view of (26) may happen only for $|i - j| \leq 1$.
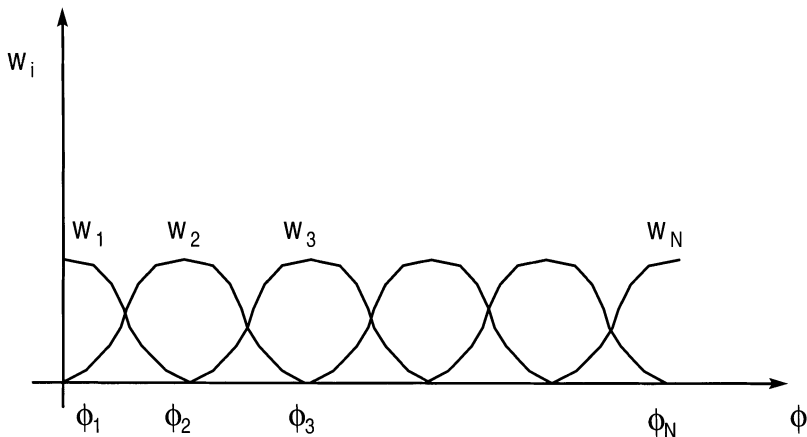
FIGURE 3   Piece-wise parabolic basis and test functions.

$f_i^{(k)}$, $[L_M^{(p,q)}]_{ij}$ by means of standard numerical integration routines appropriate for regular and singular integrands, respectively.[9]

The linear system (8) is solved numerically, e.g., using Cholesky's decomposition.[9] Due to the relatively small size of the problem ($\sim 20 \times 20$ typical), the choice of the solver does not affect appreciably the overall accuracy and CPU time.

5   COMPUTATIONAL FEATURES

In this section we discuss the main computational features of the proposed method.

The fundamental steps required for computing the Laslett coefficients can be summarized as follows:

• computation of MoM block-matrix and forcing vectors (quadrature formulas);
• solution of linear system (matrix inversion);
• computation of Laslett coefficients (derivatives).

The first task involves evaluation of $PN(N+1)/2$ double integrals for the self-interaction matrices $L_S^{(k)}$, plus $N^2P(P-1)/2$ double integrals for mutual-interaction matrices $L_M^{(p,q)}$, plus $3PN$ integrals for computing the forcing vectors c, d, f.

However, capitalizing on the possible symmetries of the structure can reduce the number of elements to compute by a factor two (stadium, cut-circle geometries) to four (rounded-corner square).

The accuracy of solutions based on Galerkin methods shows a peculiar dependance on the number N of basis-test functions used (see, e.g., Ref. 3). The accuracy increases steeply upon increasing N, until a critical value is reached. Further increasing N does *not* improve the accuracy, and may eventually lead to numerical instabilities, due to ill-conditioning of the involved matrices. In our case, the above critical value of N was ≈ 20 (five basis functions per rounded corner), *independent* of the pipe size, due to our judicious choice of Green's and basis-test functions. Storage and CPU requirements are thus very mild.

Note that the MoM matrix *does not* depend on the line source position. Hence, computation of Laslett coefficients at different points *does not* require a new computation and inversion of the block matrix $[L]$, while requiring only re-computation of the forcing vectors c, d, f.

The most attractive feature of the proposed algorithm, however, resides in our opinion in the possibility of computing Laslett coefficients in an analytical–numerical hybrid scheme. This is related to the feature, typical of the Galerkin version of MoM, of yielding an *analytic* (though approximate) solution of the Poisson problem, featuring the correct singular behavior. All further manipulations needed to compute the Laslett coefficients, including the separation of free-space term, and the computation of derivatives up to second order, can thus be performed *analytically*. This is obviously *impossible* in standard numerical approaches based on finite-elements or finite-difference methods, which, as a consequence exhibit worse accuracy and longer computing time.

6 NUMERICAL RESULTS

In order to check the accuracy of the proposed method we compared our results with the exact analytical ones available for the circular cross section geometry. In Figure 4 the percent errors are displayed for both the incoherent and coherent Laslett coefficients as functions of the scaled radial distance $\bar{\rho} = (2/a)[(x - a/2)^2 + (y - a/2)^2]^{1/2}$, $a/2$ being the pipe radius, and $(a/2, a/2)$ the pipe center. The agreement is very good.
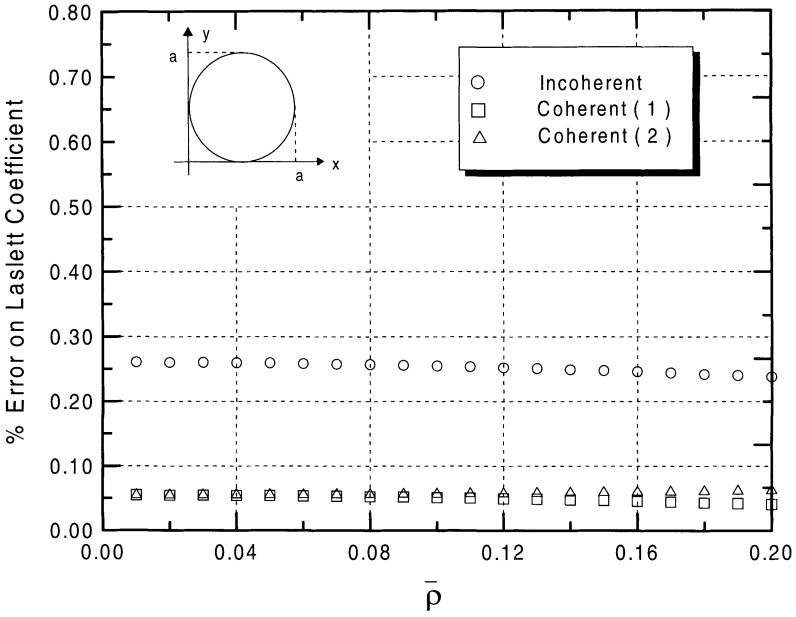
FIGURE 4 Circular pipe. Percent error on incoherent and coherent Laslett coefficient vs. scaled radial distance, $\bar{\rho} = (2/a)[(x - a/2)^2 + (y - a/2)^2]^{1/2}$.

The results obtained for a number of different geometries (square with rounded corners, stadium and cut-circle) relevant to LHC are collected in Figures 5–13.

For the square pipe with rounded corners, we confirm a number of results valid for the sharp-corner case,[10,11] viz.: (i) the square geometry has a smaller coherent tune-shift as compared to the circular one; (ii) this holds true in the coherent case at $\theta = 0$ and for both the incoherent and coherent cases at $\theta = \pi/4$. The incoherent and coherent (both normal modes) Laslett coefficients as functions of the rounded-corners (equal) radii, for several angular positions θ and for $\bar{\rho} = 0.1$ are shown in Figures 5–7. In the coherent case the influence of the rounded-corners radius is almost negligible, while in the incoherent case the Laslett coefficients along the diagonal are manifestly smaller than in any other direction, and do vanish for some value of the corners' radii.

The incoherent and coherent (both normal modes) Laslett coefficient level contours for the stadium shaped cross section geometry depicted in Figure 8, are displayed in Figures 8–10.
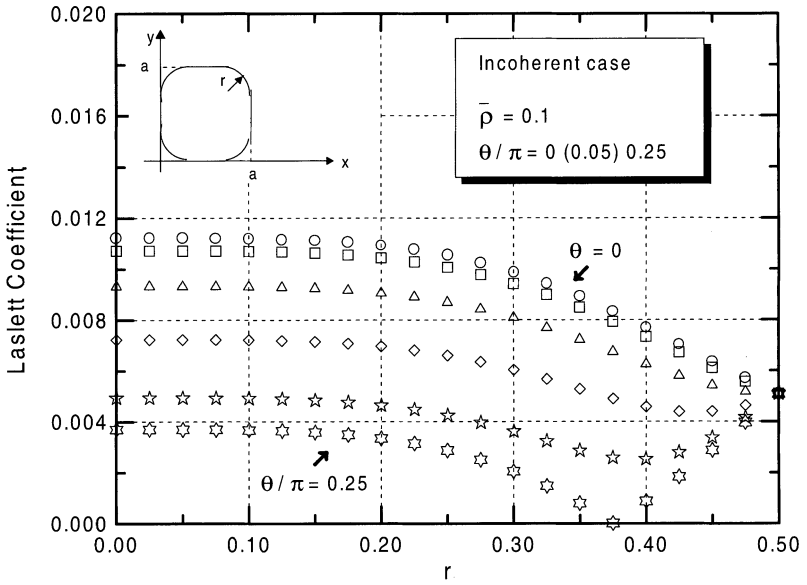
FIGURE 5 Square pipe with rounded corners ($a = 1$). Incoherent Laslett coefficient (both normal modes) vs. rounded-corner radius, at $\bar{\rho} = 0.1$, for several values of angular position, $\theta = \text{atn}[(x - 0.5a)/(y - 0.5a)]$.
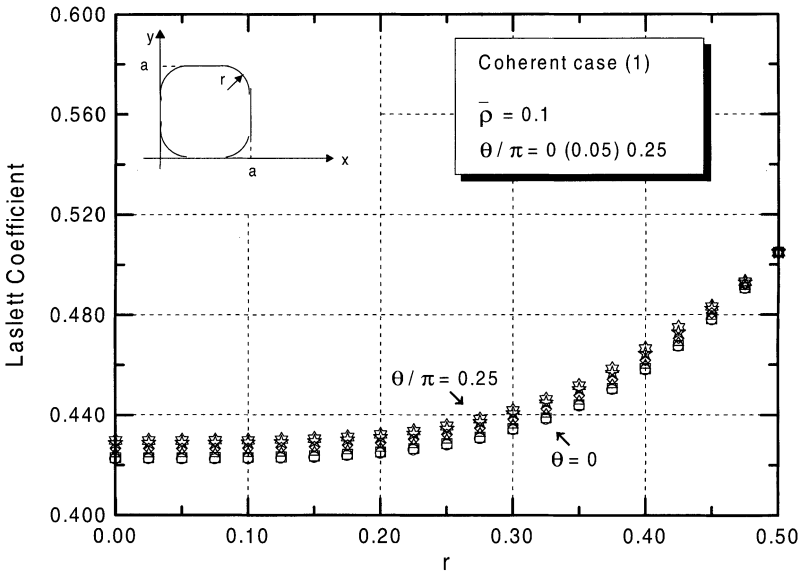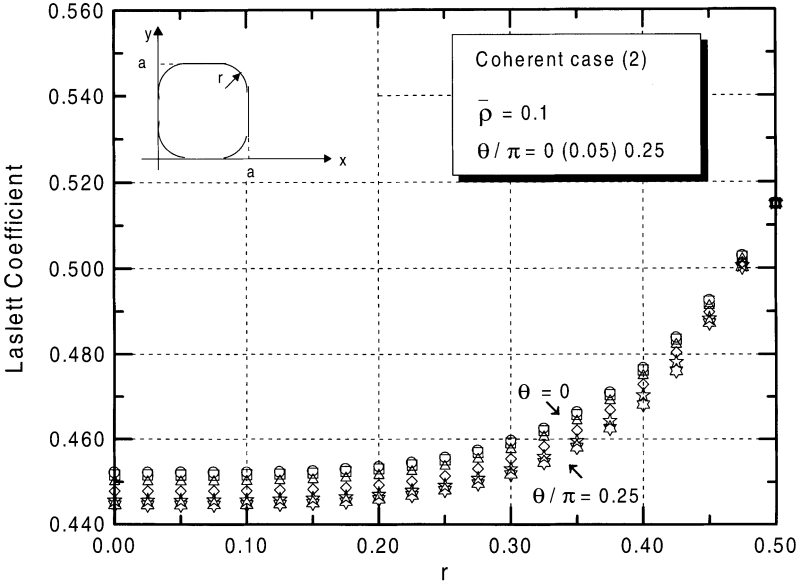

FIGURE 6 Square pipe with rounded corners ($a = 1$). Coherent Laslett coefficient (1st normal mode) vs. rounded-corner radius, at $\bar{\rho} = 0.1$, for several values of angular position.

FIGURE 7   Square pipe with rounded corners ($a = 1$). Coherent Laslett coefficient (2nd normal mode) vs. rounded-corner radius, at $\bar{\rho} = 0.1$, for several values of angular position.

For comparison, Figures 11–13 refer to the cut-circle geometry sketched in Figure 11.

7   CONCLUSIONS AND RECOMMENDATIONS

A novel approach for computing Laslett coefficients for rounded rectangular geometries with perfectly conducting pipe walls has been presented.

The algorithm is based upon a clever implementation of MoM, which leads to a small-size linear matrix problems. Comparison with known solutions and analysis of computational features indicate that the proposed method is fairly accurate and fast.

The incoherent and coherent Laslett coefficients for a number of geometries relevant to LHC have been accordingly computed.

More or less obvious extensions include the computation of magnetic Laslett coefficients, and imperfectly conducting walls.
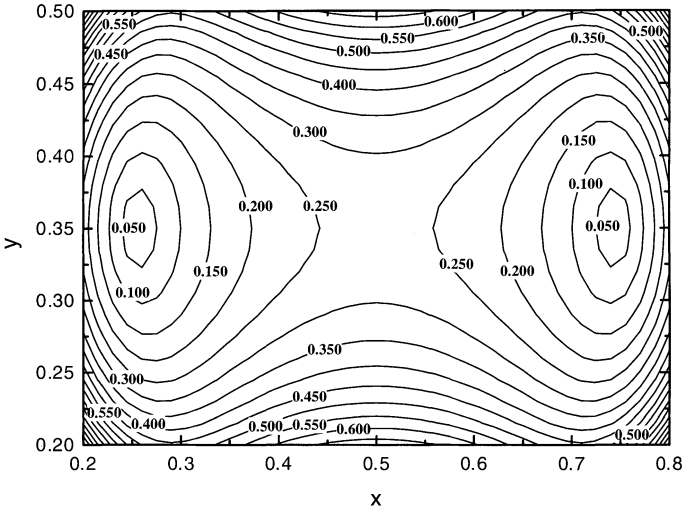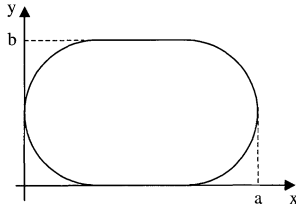
FIGURE 8 Stadium-shaped pipe. Incoherent Laslett coefficient (both normal modes). Contour lines ($a = 1$, $b = 0.7$, $0.2 \leq x \leq 0.8$, $0.2 \leq y \leq 0.5$).
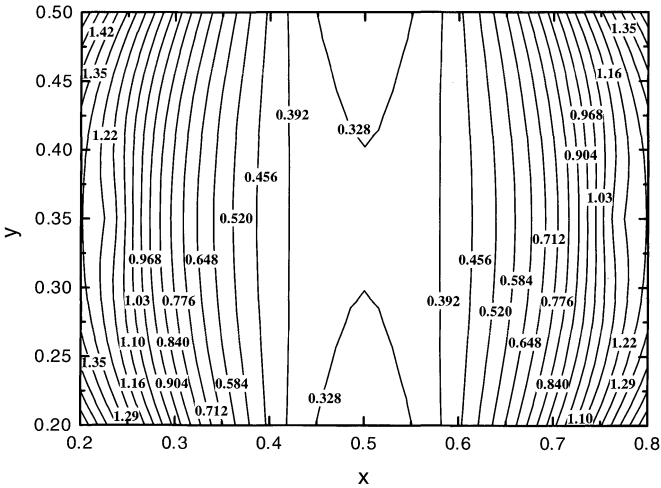

FIGURE 9 Stadium-shaped pipe. Coherent Laslett coefficient (1st normal mode). Contour lines ($a = 1$, $b = 0.7$, $0.2 \leq x \leq 0.8$, $0.2 \leq y \leq 0.5$).
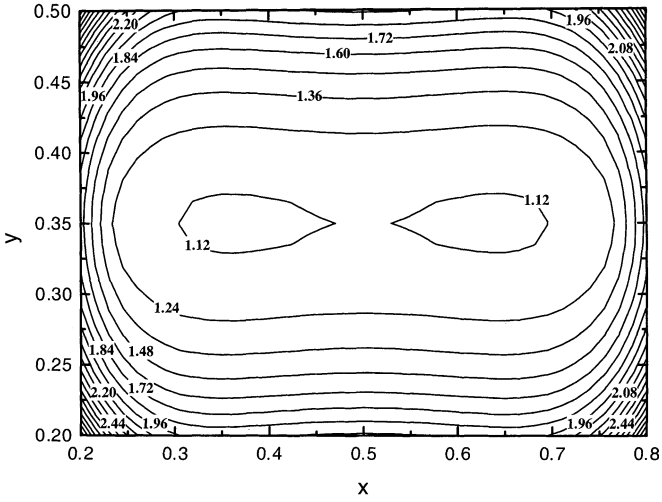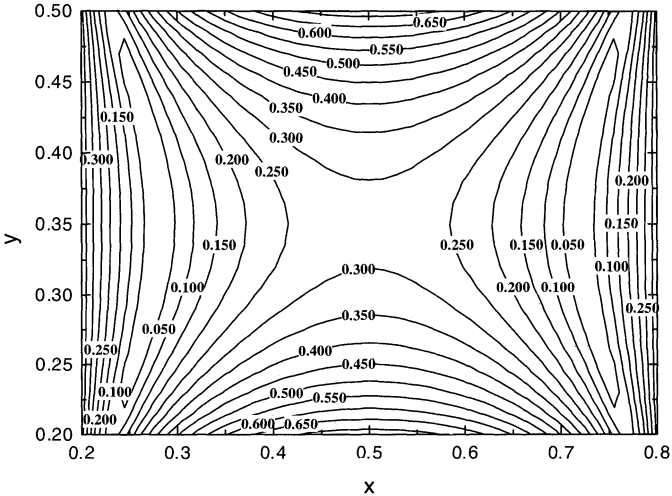
FIGURE 10 Stadium-shaped pipe. Coherent Laslett coefficient (2nd normal mode). Contour lines ($a = 1$, $b = 0.7$, $0.2 \leq x \leq 0.8$, $0.2 \leq y \leq 0.5$).
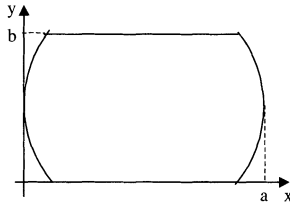

FIGURE 11 Cut-circle-shaped pipe. Incoherent Laslett coefficient (both normal modes). Contour lines ($a = 1$, $b = 0.7$, $0.2 \leq x \leq 0.8$, $0.2 \leq y \leq 0.5$).
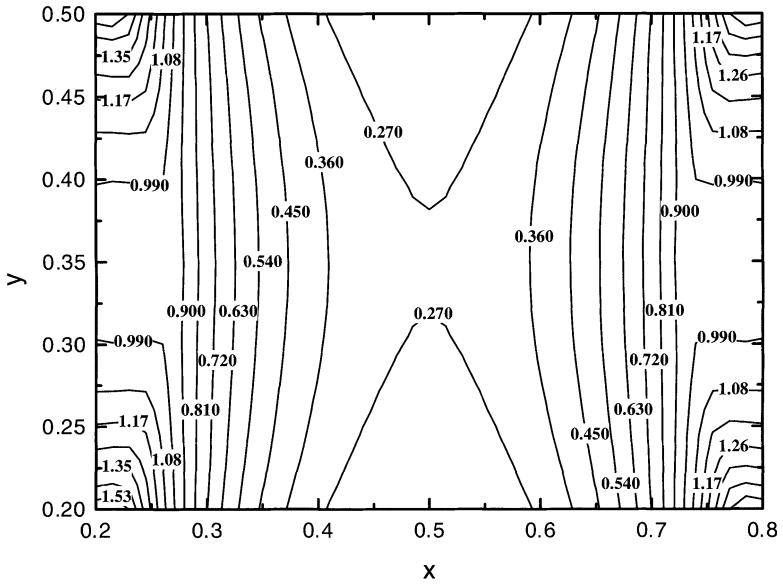
FIGURE 12 Cut-circle-shaped pipe. Coherent Laslett coefficient (1st normal mode).
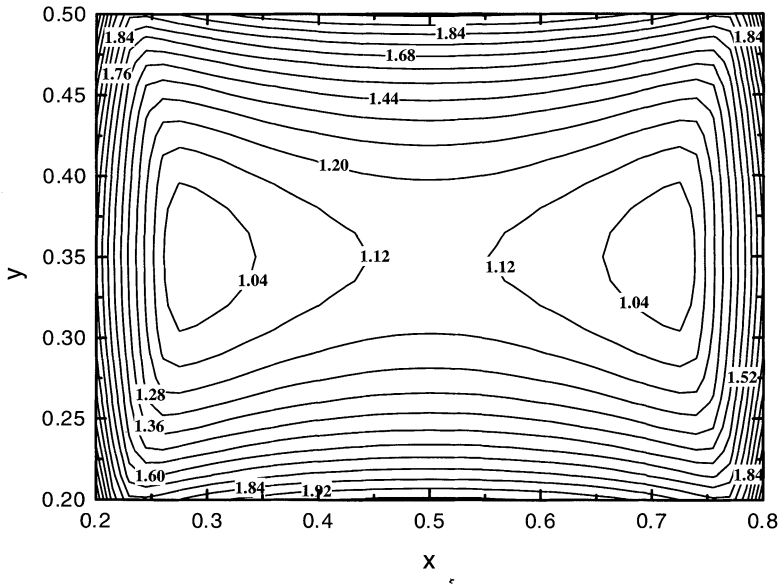Contour lines ($a = 1$, $b = 0.7$, $0.2 \leq x \leq 0.8$, $0.2 \leq y \leq 0.5$).

FIGURE 13 Cut-circle-shaped pipe. Coherent Laslett coefficient (2nd normal mode).
Contour lines ($a = 1$, $b = 0.7$, $0.2 \leq x \leq 0.8$, $0.2 \leq y \leq 0.5$).

APPENDIX A – RAPIDLY CONVERGING EXPANSION OF RDGF

The scalar (static) Green's function for the rectangular geometry is considered. The well-known eigenfunctions expansion[5]

$$g_R(r, r_b) = -4\pi \sum_{m=1}^{\infty} \frac{\psi_m(r)\psi_m(r_b)}{k_m^2}, \tag{A1}$$

$$\psi_m(r) = \frac{2}{\sqrt{ab}} \sin\left(\frac{m\pi}{a}x\right) \sin\left(\frac{m\pi}{b}y\right), \tag{A2}$$

$$k_m^2 = \left(\frac{m\pi}{a}\right)^2 + \left(\frac{m\pi}{b}\right)^2, \tag{A3}$$

is slowly convergent, especially close to the source point. Using Poisson's transformation,[13] after some lengthy algebra, the following rapidly converging series is obtained:[6,7]

$$g_R(r, r_b) = -\sum_{m=-\infty}^{\infty} \log \frac{T_m^{10}(r, r_b) T_m^{01}(r, r_b)}{T_m^{00}(r, r_b) T_m^{11}(r, r_b)}, \tag{A4}$$

where

$$T_m^{pq}(r, r_b) = 1 - 2\exp\left[|y - (-1)^p y_b + 2bm|\frac{\pi}{a}\right] \cos\left[\frac{\pi}{a}(x - (-1)^q x_b)\right]$$

$$+ \exp\left[-2|y - (-1)^p y_b + 2bm|\frac{\pi}{a}\right]. \tag{A5}$$

It is easily recognized that the (logarithmic) singularity of g_R appears in the T_0^{10} term. It was found that the accuracy obtained by taking the first seven terms ($m = -3, \ldots, 3$) is sufficient for all practical purposes.

APPENDIX B – RELEVANT LIMITS

We consider the *image* Green's function introduced in Section 3:

$$g^{(\text{im.})}(r, r_b) = g_R(r, r_b) - g_0(r, r_b). \tag{B1}$$

As shown in Section 3, the computation of *image* fields and their derivatives requires the evaluation of limits for $r \to r_b$ of $g^{(\text{im.})}$ and its derivatives. As previously stated, these limits involve $(\infty - \infty)$

indeterminate forms. In this appendix we outline the main steps for their computation. First, it is expedient to split the function g as follows:

$$g_R(\boldsymbol{r}, \boldsymbol{r}_b) = g_R^{(\text{reg.})}(\boldsymbol{r}, \boldsymbol{r}_b) + g_R^{(\text{sing.})}(\boldsymbol{r}, \boldsymbol{r}_b), \tag{B2}$$

where the singular term is easily recognized to be (see Appendix A)

$$g_R^{(\text{sing.})}(\boldsymbol{r}, \boldsymbol{r}_b) = -\log T_0^{10}(\boldsymbol{r}, \boldsymbol{r}_b), \tag{B3}$$

$$T_0^{10}(\boldsymbol{r}, \boldsymbol{r}_b) = 1 - 2\exp\left[-\frac{\pi}{a}|y - y_b|\right]\cos\left[\frac{\pi}{a}(x - x_b)\right]$$
$$+ \exp\left[-2\frac{\pi}{a}|y - y_b|\right]. \tag{B4}$$

By expanding $(g_R^{(\text{sing.})} - g_0)(\boldsymbol{r}, \boldsymbol{r}_b)$ in Taylor's series around $\boldsymbol{r} = \boldsymbol{r}_b$ we obtain

$$g_R^{(\text{sing.})}(\boldsymbol{r}, \boldsymbol{r}_b) - g_0(\boldsymbol{r}, \boldsymbol{r}_b)$$
$$\approx 2\log\left(\frac{\pi}{a}\right) + \frac{\pi|y - y_b|}{a} + \frac{\pi^2[(x - x_b)^2 - (y - y_b)^2]}{12a^2}$$
$$+ \frac{\pi^4[(x - x_b)^4 + (y - y_b)^4]}{1440a^4} - \frac{\pi^4(x - x_b)^2(y - y_b)^2}{240a^4} + \mathcal{O}(\Delta^6),$$
$$\tag{B5}$$

where $\Delta \sim (x - x_b) \sim (y - y_b)$. The singular limits needed to evaluate the *image* fields and their derivatives can be now readily computed.

References

[1] L.J. Laslett, *Proc. of the 1963 Summer Study* BNL 7534.
[2] The LHC study group, CERN/AC/95-05 (LHC), 1995.
[3] R.F. Harrington, *Field Computation by Moment Methods*, McMillan, New York, 1968.
[4] http://www.slap.cern.ch/collective/oda/BINP-codes.html.
[5] R.E. Collin, *Field Theory of Guided Waves*, 2nd ed., IEEE Press, Piscataway, 1991.
[6] M. Bressan and G. Conciauro, *Alta Frequenza* (special issue on Applied Electromagnetics), **52**, 188–190, 1983.
[7] P. Arcioni, M. Bressan and G. Conciauro, *Alta Frequenza*, **57**, 217–226, 1988.
[8] S. Petracca, CERN Rept. SL/93-13 (AP).
[9] SLATEC Public Domain Mathematical Library, distributed by NETLIB, http://www.netlib.org.
[10] S. Petracca, *Part. Acc.*, **48**, 181–192, 1994.
[11] S. Petracca, V. Galdi and I.M. Pinto, CERN Rept. SL/99-XX (AP) (in print).
[12] R.E. Collin, *ibidem*, ch. 12.